IEEE Access
Multidisciplinary | Rapid Review | Open Access Journal

Received July 2, 2018, accepted August 20, 2018, date of publication August 31, 2018, date of current version September 21, 2018.

Digital Object Identifier 10.1109/ACCESS.2018.2868238

A New Approach to Design a Broadband Doherty Power Amplifier via Dual-Transformation Real Frequency Technique

FAN MENG[1], (Student Member, IEEE), XIAO-WEI ZHU[1], (Member, IEEE), JING XIA[2], (Member, IEEE), AND CHAO YU[1], (Member, IEEE)

[1]State Key Laboratory of Millimeter Waves, Southeast University, Nanjing 210096, China
[2]School of Computer Science and Communication Engineering, Jiangsu University, Zhenjiang 212013, China

Corresponding author: Xiao-Wei Zhu (xwzhu@seu.edu.cn)

This work was supported in part by the National Science Foundation of China under Grant 61631021, Grant 61601117, and Grant 61701199, and in part by the Natural Science Foundation of Jiangsu Province of China under Grant BK20150528.

ABSTRACT A novel dual-transformation simplified real frequency technique is proposed in this paper to synthesize a broadband Doherty power amplifier (DPA). The proposed method can realize the co-design of the carrier and peaking output matching networks to achieve dual-impedance transformation at back-off (BO) and saturation simultaneously. To realize this method, a generalized driving point function with different loads of the matching network is proposed, and weight factors are adopted to combine the separate target functions to form a united one. Compared with conventional designs, no initial guess is required and additional compensating lines are eliminated to improve the performance of the DPA. Based on the proposed technique, a broadband DPA is designed and fabricated across 2.2–3.7 GHz (51% fractional bandwidth). The measurement results show that the designed DPA has a 6-dB BO efficiency of 45%–53% and a saturated output power of 43–44.6 dBm over 1.5 GHz bandwidth. Various modulated signals including 80-MHz long-term evolution-advanced signal and concurrent dual-band signal are employed to validate the DPA. In this way, the DPA can achieve an average efficiency of 45.3%–55.9% at 6.5-dB BO with the adjacent channel leakage ratio levels better than −48.6 dBc by utilizing digital predistortion.

INDEX TERMS Broadband amplifiers, Doherty power amplifiers (DPAs), dual-impedance transformations, power amplifiers, real frequency technique.

I. INTRODUCTION

With the development of ever-increasing data rate and connections for 5^{th} generation of mobile communication network (5G), the modulated signals have wider bandwidths (BWs). However, because the frequency spectrum resources around 2 GHz have been almost used up by previous generations of systems, the forthcoming commercialized 5G's candidate frequency bands have been shifted to higher frequencies, such as 2.6 GHz and 3.5 GHz [1] to achieve wider bandwidth. Meantime, the peak-to-average power ratios (PAPRs) of the transmitted signal become much higher with the evolution of the communication systems. Power amplifiers (PAs), regarded as one of the most important cells in the wireless communication systems, are required to maintain high efficiency under this new circumstance.

To resolve this issue, Doherty power amplifier (DPA) has been proposed as an effective solution to handle the modulated signals with higher PAPRs [2]–[9]. But in conventional design methodology, DPA is referred as narrowband architecture owing to its quarter-wave length impedance inverter after the carrier amplifier. To broaden the BW of DPA becomes a challenge for PA designers. In recent years, many researchers have focused on the DPA's BW extension method by modifying the output matching networks (OMNs) [10]–[13]. Among them, low-order matching networks [14], [15], noninfinity peaking impedances [16]–[18] and post-matching networks [19]–[21] are widely employed recently to enhance the DPA's BW. However, one of their major drawbacks is that the carrier and peaking OMNs are designed separately, regardless of their mutual influence, so that the performance of DPA is usually limited.

Meanwhile, optimization techniques, such as Bayesian [22] and simplified real frequency technique (SRFT) [23] have begun to be employed to design broadband DPA.

In [23], the BW of DPA is improved by employing the SRFT optimizations in carrier and peaking OMNs' design. However, the optimizations of carrier and peaking OMNs are done separately and DPA is optimized at either back-off (BO) or saturation power level. Additional offset lines are required after the OMNs, so that the BW performance of the DPA is negatively influenced by the adjustments.

This paper proposes a novel dual-transformation SRFT (DT-SRFT) method to further improve the bandwidth of DPA by the co-design of carrier and peaking OMNs. By combining the carrier and peaking OMNs into one optimization process, the OMNs can be optimized at BO and saturation power levels simultaneously to achieve the global optimal matching condition in Doherty load modulation. The compensating (offset) lines are eliminated to improve the performance of the DPA. No initial guess is required and the OMNs can be easily synthesized by the optimized scattering parameters, which can simplify the DPA design. The detailed systematic design procedures are presented to synthesize a broadband DPA with more than 50% fractional bandwidth (FBW), which provides a validation of the proposed design methodology.

The rest of this paper is organized as follows. In Section II, the relationship of carrier and peaking OMNs is analyzed in details to derive the proposed DT-SRFT. Section III introduces the systematic design procedures for broadband DPA based on this new methodology. The measurement results and the comparisons with recently established works are shown in Section IV. Finally, the conclusion is summarized in Section V.

II. ANALYSIS OF THE PROPOSED DT-SRFT

A. REVIEW OF THE CONVENTIONAL SRFT

SRFT can effectively deal with the complex-to-complex impedance matching [24]–[26] and has been widely adopted to design broadband high-efficiency single-ended PAs [27]–[32].

For a lossless and reciprocity network constructed with commensurate transmission lines (TLs), the scattering matrix of network can be expressed as:

$$[S] = \begin{bmatrix} S_{11} & S_{12} \\ S_{21} & S_{22} \end{bmatrix} = \frac{1}{g(\lambda)} \begin{bmatrix} h(\lambda) & f(\lambda) \\ f(\lambda) & -h(-\lambda) \end{bmatrix} \tag{1}$$

where λ is the complex Richard variable which is defined as:

$$\lambda = j\tan(\beta l) = j\tan(\pi f/2f_e) \tag{2}$$

where f_e is stopband frequency specified by the designer. $h(\lambda)$ and $g(\lambda)$ are the nth order polynomials and $g(\lambda)$ is strictly the Hurwitz polynomial. $f(\lambda)$ is specified by $f(\lambda) = \lambda^q(1-\lambda^2)^{k/2}$, where k is the number of cascade commensurate TLs, q is the number of shunt-short stubs, and $n = k + q + r$ is the total number of distributed elements such that r is the number of shunt-open stubs. Required by the lossless condition, $h(\lambda)$, $g(\lambda)$ and $f(\lambda)$ are regarded by:

$$|g(\lambda)|^2 = |h(\lambda)|^2 + |f(\lambda)|^2 \tag{3}$$

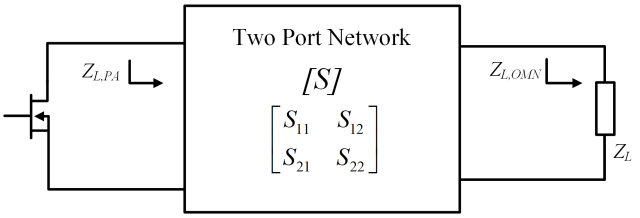

FIGURE 1. Schematic of PA's OMN.

A schematic of PA's OMN is plotted in Fig. 1. As the load impedance of transistor, $Z_{L,PA}$ is named as a driving point function (DPF) [27] to replace the conventional transfer power gain function (TPG) in SRFT [23]–[26]. For a single-ended PA, the load impedance $Z_{L,OMN}$ equals Z_0 and $Z_{L,PA}$ can be given as follows:

$$Z_{L,PA}(\lambda) = Z_0 \frac{1+S_{11}}{1-S_{11}} = Z_0 \frac{g(\lambda)+h(\lambda)}{g(\lambda)-h(\lambda)} \tag{4}$$

Here $Z_{L,PA}(\lambda)$ is a positive real function. Due to $g(\lambda)$ is strictly the Hurwitz polynomial, the solution to the $h(\lambda)$ is in real frequency domain. That means the optimized OMN constructed by the polynomials can be synthesized by distributed elements.

The SRFT optimization target is to minimize the difference between $Z_{L,PA}$ and the optimal impedance of transistor Z_{opt}. So the target function (TF) can be described as:

$$\min \Delta Z_{diff} = \sum_{i=1}^{M} \left| \frac{Z_{L,PA}(\lambda_i) - Z_{opt}(\lambda_i)}{|Z_{opt}(\lambda_i)|} \right|^2 \tag{5}$$

where M is the number of frequency points calculated in SRFT. By applying the Levenberg-Marquardt algorithm in MATLAB, the optimized scattering matrix for OMN can be solved and the distributed elements of OMN can be synthesized by Richard extraction [33].

Compared with TPG, DPF is focused on the load impedance of the transistor and can effectively distinguish the difference between $Z_{L,PA}$ and Z_{opt}. The DPF proposed in [27] cannot be adopted to DPA design directly as the load impedance of OMN varies with the input power during the load modulation in DPA design. Although SRFT has been preliminarily employed in DPA design [23], the carrier and peaking OMNs are optimized separately by the conventional TPG method and only sub-optimal solution can be obtained in the design.

B. PROPOSED DT- SRFT FOR DPA DESIGN

In order to solve these limitations, the DT-SRFT is proposed to co-design the carrier and peaking OMNs in one optimization process. A generalized DPF (G-DPF) will be derived to fulfil the co-design of the OMN, and united TF will combine the separate TFs into one process to achieve the global optimization. The DT-SRFT process will be illustrated to design the DPA in a comprehensive way.

The output architecture of DPA is shown in Fig. 2. It contains the OMNs of the carrier and peaking amplifiers and the

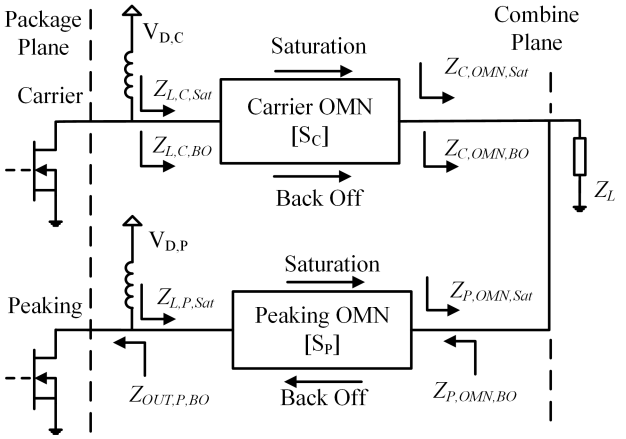

FIGURE 2. Diagram of the DPA's OMN.

load Z_L. Z_L is achieved by the post-matching network. The optimization of Z_L has been profoundly studied in [19]–[21]. At BO power level, usually the output impedance of peaking OMN $Z_{P,OMN,BO}$ is regarded as infinity in DPA analysis. However, the infinity $Z_{P,OMN,BO}$ cannot be guaranteed in broadband DPA as the phase variation of TL. The common load seen from the carrier OMN is shown as:

$$Z_{C,OMN,BO} = Z_L//Z_{P,OMN,BO} = \frac{Z_L * Z_{P,OMN,BO}}{Z_L + Z_{P,OMN,BO}} \quad (6)$$

The load impedance of carrier amplifier at BO $Z_{L,C,BO}$ can be achieved by converting $Z_{C,OMN,BO}$ through the carrier OMN. As shown in (6), $Z_{L,C,BO}$ is not only affected by Z_L, but also affected by $Z_{P,OMN,BO}$. That means the peaking OMN must be carefully designed though the peaking amplifier is OFF at BO. At saturation power level, considering the active load modulation, the load impedances of carrier and peaking OMNs are given by:

$$\begin{cases} Z_{C,OMN,Sat} = (1+\alpha)Z_L \\ Z_{P,OMN,Sat} = (1+1/\alpha)Z_L \end{cases} \quad (7)$$

where α is the current ratio between the carrier and peaking transistors at saturation. The carrier and peaking OMNs convert $Z_{C,OMN,Sat}$ and $Z_{P,OMN,Sat}$ to $Z_{L,C,Sat}$ and $Z_{L,P,Sat}$ respectively. The relationship of impedances in the DT-SRFT is summarized in Fig. 3. $Z_{opt,C,Sat}$ and $Z_{opt,P,Sat}$ are the optimal impedances of carrier and peaking amplifiers at saturation obtained from the load-pull simulation. Similarly, $Z_{opt,C,BO}$ represents the carrier amplifier's optimal load impedance at BO. These three optimal impedances are the optimized targets of DT-SRFT. At saturation, the optimizations of carrier and peaking OMNs are influenced by Z_L and α. At BO, the carrier and peaking OMNs are correlated with each other. $Z_{P,OMN,BO}$ is transformed from the output impedance of peaking amplifier $Z_{OUT,P,BO}$. DT-SRFT enrolls the two OMNs together to calculate $Z_{L,C,BO}$. $Z_{L,C,Sat}$, $Z_{L,P,Sat}$ and $Z_{L,C,BO}$ are the three G-DPFs of DT-SRFT, which should be as close to the optimal impedances of DPA

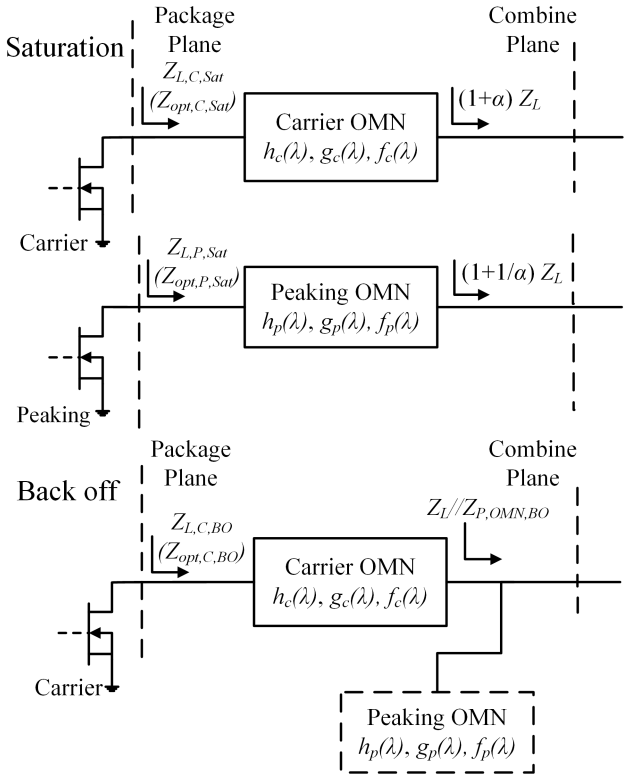

FIGURE 3. Relationship of impedances in DT-SRFT.

as possible. Besides, the carrier and peaking OMNs are required to be optimized in one process, so weight factors are introduced to combine the three transformations into one united TF.

1) CALCULATION OF $Z_{L,C,BO}$

The proposed G-DPFs will be derived in this part. The G-DPF for carrier at BO $Z_{L,C,BO}$ is calculated at first. As presented in Fig. 2, for the peaking OMN, $Z_{P,OMN,BO}$ can be expressed as follows:

$$Z_{P,OMN,BO} = Z_0 \frac{1+\Gamma_{P,OMN,BO}}{1-\Gamma_{P,OMN,BO}} \quad (8)$$

$$\Gamma_{P,OMN,BO} = S_{P,22} + \frac{S_{P,12}S_{P,21}\Gamma_{OUT,P,BO}}{1-S_{P,11}\Gamma_{OUT,P,BO}} \quad (9)$$

where $\Gamma_{OUT,P,BO} = (Z_{OUT,P,BO} - Z_0)/(Z_{OUT,P,BO} + Z_0)$. By replacing the scatter parameters with $h_p(\lambda)$, $g_p(\lambda)$ and $f_p(\lambda)$ and considering the lossless condition in (3), $Z_{P,OMN,BO}$ in Richard domain can be written as:

$$Z_{P,OMN,BO}(\lambda) = Z_0 \frac{g_p(\lambda) - h_p(-\lambda) - [h_p(\lambda) - g_p(\lambda)]\Gamma_{OUT,P,BO}(\lambda)}{g_p(\lambda) + h_p(-\lambda) - [h_p(\lambda) + g_p(\lambda)]\Gamma_{OUT,P,BO}(\lambda)} \quad (10)$$

After obtaining the expression of $Z_{P,OMN,BO}$, the load impedance of carrier OMN at BO $Z_{C,OMN,BO}$ can be calculated by (6). For the carrier OMN, the load impedance of the

transistor can be presented as follows:

$$Z_{L,C,BO} = Z_0 \frac{1+\Gamma_{L,C,BO}}{1-\Gamma_{L,C,BO}} \tag{11}$$

$$\Gamma_{L,C,BO} = S_{C,11} + \frac{S_{C,12}S_{C,21}\Gamma_{C,OMN,BO}}{1-S_{C,22}\Gamma_{C,OMN,BO}} \tag{12}$$

where $\Gamma_{C,OMN,BO} = (Z_{C,OMN,BO} - Z_0)/(Z_{C,OMN,BO} + Z_0)$. After substituting the scatter matrix of carrier OMN with $h_c(\lambda)$, $g_c(\lambda)$ and $f_c(\lambda)$, the G-DPF $Z_{L,C,BO}$ adopted in DT-SRFT is shown as:

$$Z_{L,C,BO}(\lambda) = Z_0 \frac{g_c(\lambda) + h_c(\lambda) + [h_c(-\lambda) + g_c(\lambda)]\,\Gamma_{C,OMN,BO}(\lambda)}{g_c(\lambda) - h_c(\lambda) + [h_c(-\lambda) - g_c(\lambda)]\,\Gamma_{C,OMN,BO}(\lambda)} \tag{13}$$

Compared with the conventional DPF expression in (4), the proposed G-DPF in (13) contains the reflection coefficient at the combine plane, so that it can deal with the problem when the load impedance of OMN varies.

2) CALCULATION OF $Z_{L,C,SAT}$ AND $Z_{L,P,SAT}$

Similar to the expression of $Z_{L,C,BO}$ in (13), the G-DPFs $Z_{L,C,Sat}$ and $Z_{L,P,Sat}$ can be calculated by:

$$Z_{L,C,Sat}(\lambda) = Z_0 \frac{g_c(\lambda) + h_c(\lambda) + [h_c(-\lambda) + g_c(\lambda)]\,\Gamma_{C,OMN,Sat}(\lambda)}{g_c(\lambda) - h_c(\lambda) + [h_c(-\lambda) - g_c(\lambda)]\,\Gamma_{C,OMN,Sat}(\lambda)} \tag{14}$$

$$Z_{L,P,Sat}(\lambda) = Z_0 \frac{g_p(\lambda) + h_p(\lambda) + \left[h_p(-\lambda) + g_p(\lambda)\right]\Gamma_{P,OMN,Sat}(\lambda)}{g_p(\lambda) - h_p(\lambda) + \left[h_p(-\lambda) - g_p(\lambda)\right]\Gamma_{P,OMN,Sat}(\lambda)} \tag{15}$$

where $\Gamma_{C,OMN,Sat} = (Z_{C,OMN,Sat} - Z_0)/(Z_{C,OMN,Sat} + Z_0)$ and $\Gamma_{P,OMN,Sat} = (Z_{P,OMN,Sat} - Z_0)/(Z_{P,OMN,Sat} + Z_0)$. As expressed in (7), the reflection coefficients $\Gamma_{C,OMN,Sat}$ and $\Gamma_{P,OMN,Sat}$ at the combine plane are not only related to Z_L but also related to the current ratio α.

In this way, the expressions of the three G-DPFs have been illustrated to fulfill DT-SRFT optimization. Different from conventional SRFT method in DPA design, the DT-SRFT combines the carrier and peaking OMNs together to optimize the three G-DPFs with the help of (13), (14) and (15) and the influence of peaking amplifier is enrolled into the optimization to broaden the BW of DPA.

It should be mentioned that the scatter parameters of carrier and peaking OMNs $h_c(\lambda)$ and $h_p(\lambda)$ are the optimization objects and they must maintain identical in (10), (13), (14) and (15). The united TF combines them into one optimization process to achieve the global optimal matching condition in Doherty load modulation.

3) UNITED TF IN DT-SRFT

Different from only one set of DPF in the conventional SRFT optimization, three G-DPFs are needed in DT-SRFT. Furthermore, $Z_{P,OMN,BO}$ is adopted to calculate $Z_{L,C,BO}$ as shown in (13). Hence, the complexity of DT-SRFT will be significantly increased. As the conventional TF in (5) adopted square operation, the required optimization time in DT-SRFT will be longer if the conventional one is used directly. To reduce the complexity of DT-SRFT, the modified TF is constructed as follows:

$$\min \Delta Z_{diff} = \sum_{i=1}^{M} \left[\left| \frac{Re(Z_L(\lambda_i)) - Re(Z_{opt}(\lambda_i))}{|Z_{opt}(\lambda_i)|} + \frac{Im(Z_L(\lambda_i)) - Im(Z_{opt}(\lambda_i))}{|Z_{opt}(\lambda_i)|} \right| + \right] \tag{16}$$

As shown in (16), the real and imagine part of the impedance differences are calculated separately. The square operation is replaced by the add operation. The complexity of the SRFT optimization can be reduced by this modification.

Nevertheless, the employment of G-DPF and TF are not enough for the DPA design as the optimized OMNs for each TF are different if individual SRFT procedures are used respectively. In DPA design, one process should combine the three TFs together to optimize the carrier and peaking OMNs. Therefore, to reduce the complexity of DT-SRFT, an arithmetic weight method is applied. Three weight factors β, γ and δ are introduced and they are regarded by $\beta + \gamma + \delta = 1$. Multiplied by the three factors, the united TF ΔZ_{diff} for the DT-SRFT optimization is constructed as follows:

$$\min \Delta Z_{diff,DPA} = \beta * \Delta Z_{diff,C,Sat} + \gamma * \Delta Z_{diff,C,BO} + \delta * \Delta Z_{diff,P,Sat} \tag{17}$$

where

$$\Delta Z_{diff,C,Sat} = \sum_{i=1}^{M} \left[\left| \frac{Re(Z_{L,C,Sat}(\lambda_i)) - Re(Z_{opt,C,Sat}(\lambda_i))}{|Z_{opt,C,Sat}(\lambda_i)|} + \frac{Im(Z_{L,C,Sat}(\lambda_i)) - Im(Z_{opt,C,Sat}(\lambda_i))}{|Z_{opt,C,Sat}(\lambda_i)|} \right| + \right]$$

$$\Delta Z_{diff,C,BO} = \sum_{i=1}^{M} \left[\left| \frac{Re(Z_{L,C,BO}(\lambda_i)) - Re(Z_{opt,C,BO}(\lambda_i))}{|Z_{opt,C,BO}(\lambda_i)|} + \frac{Im(Z_{L,C,BO}(\lambda_i)) - Im(Z_{opt,C,BO}(\lambda_i))}{|Z_{opt,C,BO}(\lambda_i)|} \right| + \right]$$

$$\Delta Z_{diff,P,Sat} = \sum_{i=1}^{M} \left[\left| \frac{Re(Z_{L,P,Sat}(\lambda_i)) - Re(Z_{opt,P,Sat}(\lambda_i))}{|Z_{opt,P,Sat}(\lambda_i)|} + \frac{Im(Z_{L,P,Sat}(\lambda_i)) - Im(Z_{opt,P,Sat}(\lambda_i))}{|Z_{opt,P,Sat}(\lambda_i)|} \right| + \right]$$

The weight factors β, γ and δ must be intensively selected in the design. The choices of these coefficients are determined by the sensitivity of the optimal impedance for each state. If the TF $\Delta Z_{diff,C,BO}$ leads to more output power and

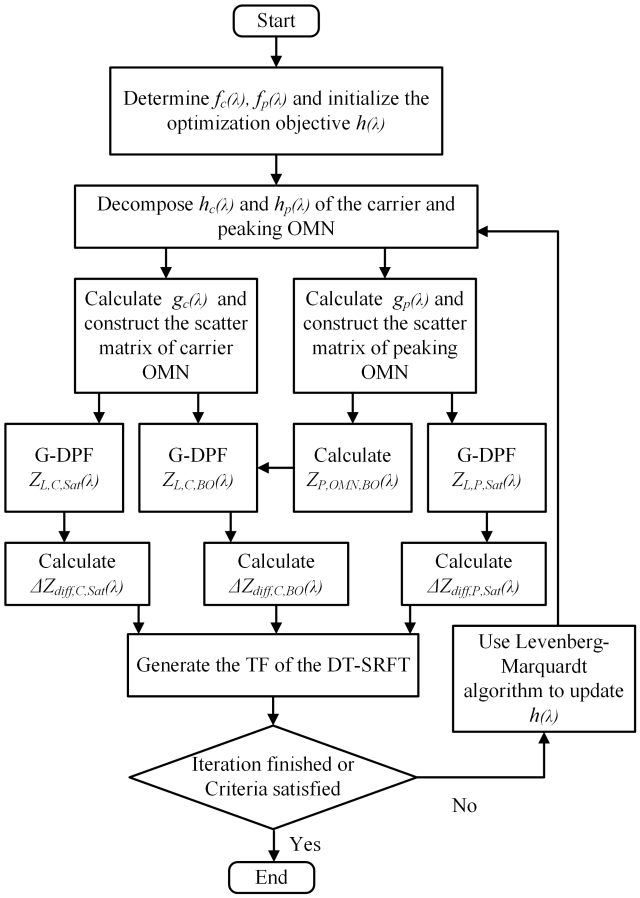

FIGURE 4. Proposed DT-SRFT process of DPA design.

efficiency degradation than $\Delta Z_{diff,C,Sat}$ and $\Delta Z_{diff,P,Sat}$, γ should be close to 1 and $Z_{L,C,BO}$ will be closer to $Z_{opt,C,BO}$ after the DT-SRFT optimization.

4) DT-SRFT PROCESS OF DPA'S OMN DESIGN

After the G-DPFs and united TF have been derived, the DT-SRFT process of DPA's OMN design is illustrated in Fig. 4. Dual-impedance transformation is achieved by this optimization. The carrier and peaking OMNs are combined together so that the comprehensive optimal load impedance of the DPA will be approached by this method. The details are included in the following steps:

(1) According to the structure of the carrier and peaking OMNs, $f_c(\lambda)$ and $f_p(\lambda)$ are determined and the optimization object $h(\lambda)$ is initialized. The limited tolerance and iteration number are also required to terminate the process.

(2) The $h(\lambda)$ is decomposed by $h_c(\lambda)$ and $h_p(\lambda)$ for the carrier and peaking OMNs. In the theory of lossless and reciprocity network, $g(\lambda)$ can be calculated by $f(\lambda)$ and $h(\lambda)$. The scatter matrices of carrier and peaking OMNs can be constructed with these polynomials.

(3) Z_L is determined by the post-matching network of DPA. According to Z_L and α, the DPFs $Z_{L,C,Sat}$ and $Z_{L,P,Sat}$ can be calculated by (14) and (15). The output impedance of peaking amplifier at BO $Z_{OUT,P,BO}$ can be obtained by the S-parameter simulation. $Z_{P,OMN,BO}$ should be calculated first by (10). $Z_{P,OMN,BO}$ is then adopted to (6) to obtain $Z_{C,OMN,BO}$. With Z_L and $Z_{C,OMN,BO}$, the G-DPF $Z_{L,C,BO}$ can be calculated by (13).

(4) Using the three G-DPFs $Z_{L,C,Sat}$, $Z_{L,C,BO}$ and $Z_{L,P,Sat}$, the TFs for each state can be calculated by (16). Multiplied by the weight factors, the three TFs are summed together. The united TF $\Delta Z_{diff,DPA}$ for DT-SRFT can be obtained. The Levenberg-Marquardt algorithm in MATLAB is used to minimize $\Delta Z_{diff,DPA}$ and update the optimization object $h(\lambda)$.

(5) The steps (2)-(4) are repeated. The minimum $\Delta Z_{diff,DPA}$ can be acquired when the limited tolerance or iteration number is reached.

The comprehensive optimal load impedances of carrier and peaking transistors can be obtained with the specific OMN structures and the stopband frequencies. The optimization effects are varied with the number of TLs (OMN structure) and length of each TL (stopband frequency). In order to achieve the best performance of the broadband DPA, further parameter sweeps should be adopted to search for the optimal structures and stopband frequencies for carrier and peaking OMNs.

III. IMPLEMENTATION OF BROADBAND DPA VIA DT-SRFT

In section II, the theory of the G-DPF and TF have been derived and the process of DT-SRFT has been illustrated to design the broadband DPA. In this section, a systematic design procedure is presented for a 2.2-3.7 GHz symmetrical broadband DPA by DT-SRFT optimization to obtain the optimal efficiency at 6-dB BO. The DPA can cover the upcoming 5G's candidate frequency bands and be compatible with the traditional long term evolution (LTE) bands.

A. THE SELECTION OF OPTIMAL IMPEDANCE

Two Wolfspeed's GaN transistors CGH40010F are used to verify the methodology. The DT-SRFT procedures are operated in MATLAB and circuit simulations are conducted in Keysight ADS with large signal device model provided by the vendor.

The carrier amplifier is biased at class-AB mode whose quiescent current is 50 mA. The gate voltage of the peaking amplifier is set to −6.5 V, corresponding to the class-C mode. The drain voltage is set to 26 V and 30 V for the carrier and peaking devices respectively to ensure the identical current at saturation. The regular selection of Z_L in symmetrical DPA design is adopted. In this way, α equals 1 and Z_L equals 25 Ω for the following design.

Five frequencies of 2.2, 2.6, 3, 3.3 and 3.7 GHz are selected to represent the frequency response for the entire frequency band of 2.2-3.7 GHz. Load-pull and source-pull simulations are intensively performed to find the optimal fundamental

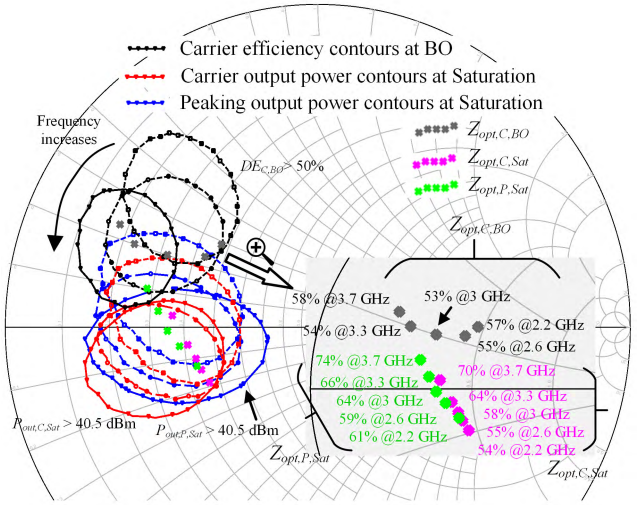

FIGURE 5. Output power and efficiency contours and the selected optimal impedances of carrier and peaking transistors.

impedances. As shown in Fig. 5, the carrier efficiency contours at BO represent the area with higher than 50% drain efficiency (DE). The output power regions for the carrier and peaking at saturation achieved greater than 40.5 dBm are also given on the Smith Chart. The contours are depicted with the frequency of 2.2, 3 and 3.7 GHz respectively. In addition, the optimal load impedances of the carrier and peaking transistors selected in DT-SRFT are also marked within the efficiency and power contours. In order to clarify the choice of the optimal load impedances, the impedances' distributions are highlighted. The impedance $Z_{opt,C,BO}$ is simulated at 6-dB BO (37 dBm) and $Z_{opt,C,Sat}$ and $Z_{opt,P,Sat}$ are simulated at saturation (40.5 dBm). The DEs with the corresponding frequencies are given in Fig. 5. The variation of the optimal impedances from low to high frequencies is clockwise according to construction of OMN so that the DT-SRFT can perform well at each frequency. The output impedances of peaking amplifier at BO are achieved by the small signal S-parameter simulation in ADS. The optimal and output impedances adopted in this design are listed in Table 1.

TABLE 1. Optimal impedances of carrier and peaking transistors.

Frequency	$Z_{opt,C,Sat}$ (Ω)	$Z_{opt,C,BO}$ (Ω)	$Z_{opt,P,Sat}$ (Ω)	$Z_{OUT,P,BO}$ (Ω)
2.2GHz	23.1-j*9.3	28+j*18.4	21.6-j*6.2	0.5-j*39.5
2.6GHz	22.2-j*6.9	25.6+j*11.5	19.2-j*2.8	0.6-j*29.5
3.0GHz	21.6-j*5	22+j*10	17.5-j*0.5	0.5-j*22.8
3.3GHz	20.5-j*2.7	18.4+j*10.5	16.1+j*2.2	0.5-j*18.8
3.7GHz	18.2+j*1.7	15+j*13.5	14.3+j*5	0.9-j*14.4

B. DT-SRFT OPTIMIZATION FOR THE OMNS OF DPA

The proposed DT-SRFT is adopted to optimize the carrier and peaking OMNs. The procedure of the design is shown in Fig. 6. The detailed steps are illustrated as follows:

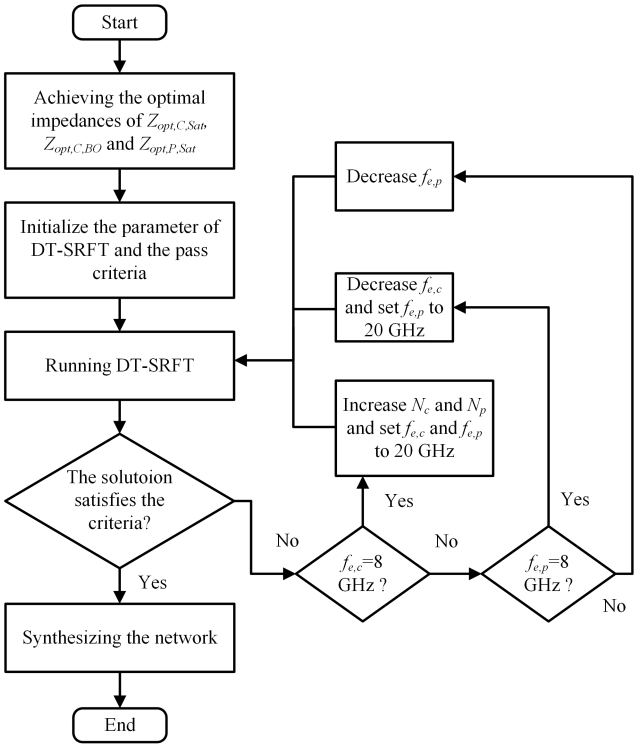

FIGURE 6. Design procedure of the OMNs of DPA by employing DT-SRFT.

First of all, after obtaining the optimal impedances $Z_{opt,C,Sat}$, $Z_{opt,C,BO}$ and $Z_{opt,P,Sat}$, the parameters of DT-SRFT should be initialized. At first, scouting the contours in Fig. 5, the efficiency contours are smaller than the output power contours and enhancing the DE at BO is the first priority in DPA design. So the weight factor γ is set to 0.4 to ensure the optimization effect of $Z_{opt,C,BO}$, and the weight factors β and δ for $Z_{opt,C,Sat}$ and $Z_{opt,P,Sat}$ are both equal to 0.3 because carrier and peaking amplifiers deliver the same output power at saturation in symmetrical DPA. Then, low-order MNs are widely used to extend DPA's BW recently [14]. To apply the low-order MNs, less number of distributed elements N and higher stopband frequency f_e are preferred. The initial N and f_e of the carrier and peaking OMNs are set to 1 and 20 GHz. Lastly, the passing criteria of DT-SRFT is to limit the maximum of the target function under 0.4 after observing the sensitivity of power and efficiency contours.

Secondly, with the initialized N_c, N_p, $f_{e,c}$ and $f_{e,p}$, the process of DT-SRFT shown in Fig. 4 is operated with specific OMN structures and stopband frequencies. The solution to the optimization will be updated by changing the parameters of the DT-SRFT. If the criteria are not satisfied after DT-SRFT process, the stopband frequency of peaking OMN $f_{e,p}$ will be decreased at first. Then, if $f_{e,p}$ is decreased to 8 GHz and the solution still does not meet the criteria, the stopband frequency of carrier OMN $f_{e,c}$ will be reduced and $f_{e,p}$ will return to 20 GHz.

Thirdly, after traversing the $f_{e,c}$ and $f_{e,p}$, the structure of OMN will be modified. Similar processes by increasing the

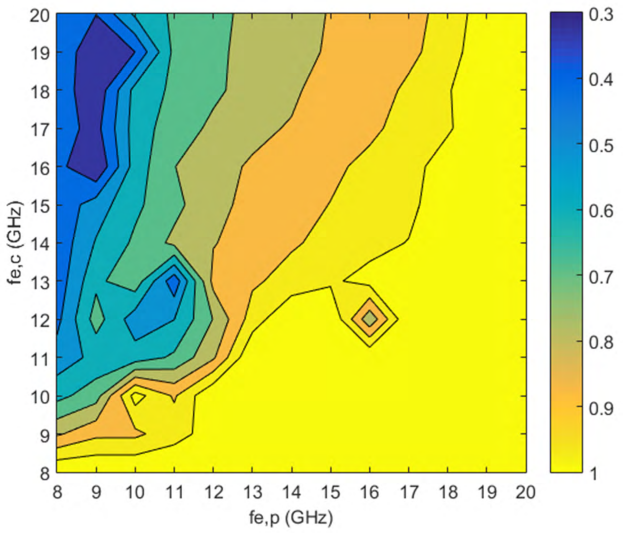

FIGURE 7. Result of the united target function calculated by DT-SRFT of the DPA design.

distributed elements of carrier and peaking OMNs N_c and N_p are repeated to search for the best solution of the DT-SRFT.

Last but not least, if the criteria are satisfied, the OMNs of carrier and peaking amplifiers are synthesized by Richard extraction or other synthesis method.

After the procedure of broadband DPA design is operated, the calculated united TF $\Delta Z_{diff,DPA}$ of the procedure is presented in Fig. 7. Two and four cascade commensurate TLs are selected as the OMNs of carrier and peaking amplifiers respectively. When $f_{e,p}$ equals 9 GHz and $f_{e,c}$ is between 16 and 19 GHz, $\Delta Z_{diff,DPA}$ is below 0.4, as shown in Fig. 7. After examining $\Delta Z_{diff,DPA}$ carefully, the stopband frequencies of carrier OMNs $f_{e,c}$ and $f_{e,p}$ are chosen as 16 GHz and 9 GHz. The $h(\lambda)$ and $g(\lambda)$ of the carrier and peaking OMNs calculated by the DT-SRFT optimization are given as presented:

$$h_c(\lambda) = 2.319\lambda^2 - 1.504\lambda \quad (18)$$

$$g_c(\lambda) = 2.523\lambda^2 + 3.052\lambda + 1 \quad (19)$$

$$h_p(\lambda) = 2.034\lambda^4 - 1.004\lambda^3 - 1.506\lambda^2 - 1.472\lambda \quad (20)$$

$$g_p(\lambda) = 2.266\lambda^4 + 6.936\lambda^3 + 8.158\lambda^2 + 4.742\lambda + 1 \quad (21)$$

The scattering parameters of carrier and peaking OMNs can be calculated by (1) and (3) with the obtained $h(\lambda)$ and $g(\lambda)$. Then by using the Richard extraction, the synthesized carrier and peaking OMNs are shown in Fig. 8. The characteristic impedances of the OMNs are 64.1 Ω and 13.2 Ω for carrier and 42.2 Ω, 16.8 Ω, 65.9 Ω and 38.5 Ω for peaking. The quarter-wave length at the stopband frequencies $f_{e,c}$ and $f_{e,p}$ is the length of each TL respectively. The simulated frequency response of the OMNs are also presented in Fig. 8. Compared with the selected optimal impedances shown in Fig. 5, the simulation results show that the OMNs designed by the proposed DT-SRFT can achieve a good matching required by a broadband DPA.

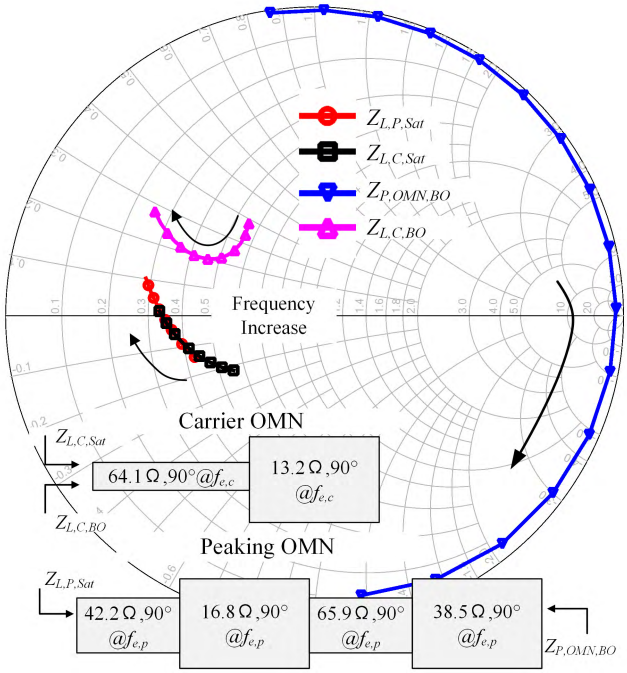

FIGURE 8. Simulated load impedances of the transistors and the synthesized carrier and peaking OMNs.

TABLE 2. Calculated target functions with different weight factors.

Weight Factors (β, γ, δ)	$\Delta Z_{diff,C,Sat}$	$\Delta Z_{diff,C,BO}$	$\Delta Z_{diff,P,Sat}$
(0.3, 0.4, 0.3)	0.671	0.232	0.132
(0.2, 0.4, 0.4)	0.793	0.211	0.121
(0.4, 0.2, 0.4)	0.610	0.320	0.105
(0.3, 0.5, 0.2)	0.688	0.158	0.579

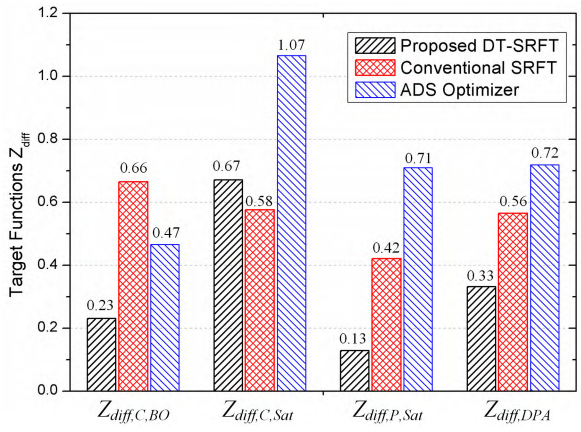

FIGURE 9. Impedance differences of the broadband DPA by DT-SRFT and comparison with conventional SRFT and ADS simulation results.

In order to obtain the appropriate weight factors of the DT-SRFT optimization, additional three sets of weight factors are also adopted in the DT-SRFT design procedure. After the procedure is operated, the calculated TFs with different weight factors are summarized in Table 2. Employing the

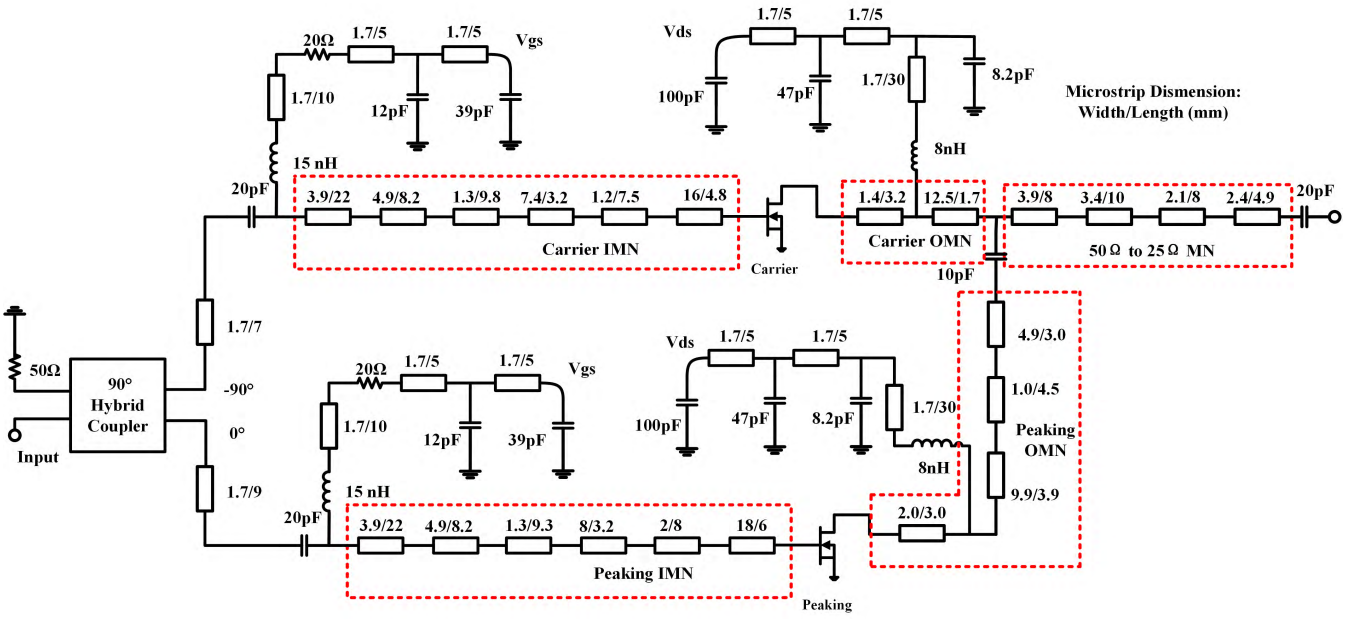

FIGURE 10. Schematic of the designed DPA fabricated on Taconic RF35 substrate with 30 mil thickness.

selected weight factors (0.3, 0.4, 0.3), the calculated TFs are 0.671, 0.232 and 0.132. Once one weight factor is set to 0.2, it leads dreadful increacement for the corresponding TF and large difference from the optimal impedance. In this way, the weight factors (0.3, 0.4, 0.3) are suitable in this broadband DPA design.

Furthermore, the TFs $\Delta Z_{diff,C,Sat}$, $\Delta Z_{diff,C,BO}$, $\Delta Z_{diff,P,Sat}$ and the united TF $\Delta Z_{diff,DPA}$ calculated by (16) and (18) are shown in Fig. 9. According to Fig. 9, it can be concluded that DT-SRFT can minimize the TFs at BO and saturation simultaneously. For comparison, the conventional SRFT in [23] and the algorithm of gradient in Keysight ADS optimizer are also adopted to optimize the desired impedances expressed in Table 1. The structure of OMNs are the same with the proposed DPA. The conventional SRFT are used to optimize the desired impedance at saturation and additional offset line is needed to adjust the load impedance at BO. The corresponding calculated TFs are also depicted in Fig. 9. Clearly, the proposed DT-SRFT performs better than the ADS optimizer as the performance of the ADS optimizer is limited by the large amount of the optimization goals [22]. The BO performance of the conventional SRFT gets suffered as the optimizations are operated at saturation and the relationship between carrier and peaking OMNs at BO is neglected in conventional SRFT.

C. SYSTEM SIMULATION

After determining the OMNs, the full circuit of the proposed DPA can be built, as shown in Fig. 10. The substrate used is Taconic RF35 with a thickness of 30 mil and a dielectric constant of 3.5. A 90° hybrid coupler 11306-3S from Anaren is used as the input signal splitter to ensure the equal input power and a 90° phase shift over a wide frequency range. The drain and the gate of the transistor are both fed by inductors. An 8nH inductor A03T from Coilcraft is used in drain bias circuit, and a 15 nH inductor LQW18AN15N from Murata is used at gate of the transistor. As the width of the first TL is limited by the package wing of the transistor, the OMNs of carrier and peaking are slightly modified by ADS Optimization. Due to the load impedances of the input matching networks (IMNs) and output combiner are pre-determined in this design, a sixth-order stepped-impedance matching topology is used to design the IMNs over 2.2-3.7 GHz and a fourth-order Chebyshev's impedance transformer centered at 3 GHz with 60% FBW is used as the output combiner.

The simulated DE and gain results of the designed DPA are presented in Fig. 11. The saturation output power of

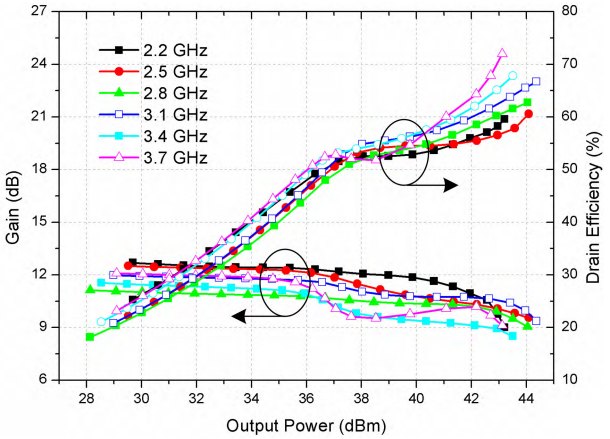

FIGURE 11. Simulation results of the designed broadband DPA.

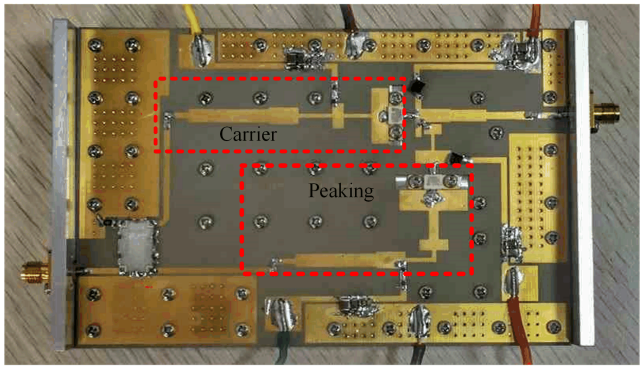

FIGURE 12. Photograph of the fabricated DPA.

the proposed DPA is 43.1-44.5 dBm within the entire frequency band. The DEs are 50.6%-53.2% at 6-dB BO and 59.6%-67.8% at saturation. The gain is around 11 dB at 6-dB BO over 2.2-3.7 GHz. These results show that a broadband DPA can be designed by the DT-SRFT proposed in this paper.

IV. MEASURED RESULTS

Based on the designed schematics, a broadband DPA was fabricated on Taconic RF35 substrate used in the simulation, as shown in Fig. 12. Continuous wave (CW) and modulated signal measurements were carried out over 2.2-3.7 GHz to verify the performance of the designed broadband DPA.

A. CW MEASUREMENTS

CW measurements were utilized to evaluate the efficiency, output power and gain characters of the fabricated DPA using Rohde & Schwarz SMW200A vector signal generator and N9030A PXA signal analyzer from Keysight.

Fig. 13 shows the measured gain and DE versus output power corresponding to the designed frequencies. Pronounced Doherty behavior is achieved by the fabricated broadband DPA.

To clearly observe the performances of the fabricated DPA, the frequency response of the measured DE, saturated output power and gain are summarized in Fig. 14. The Measured DE ranges from 54.5% to 68.7% at saturation and 45.0% to 52.8% at 6-dB BO across 2.2-3.7 GHz. The saturation output power is 43-44.6 dBm. The gain at 6-dB BO varies from 10.1 dB to 11.8 dB. For comparison, the simulation results are also plotted in Fig. 14. The comparison shows that the measured results have a good agreement with the simulation results.

A comparison between the performance of the designed DPA and recently established DPAs are summarized in Table 3. Compared with the most broadband design [11], higher power utilization factor (PUF) and DE at 6-dB BO and saturation are obtained by the proposed DPA. Compared with [10], [14], and [16], this work presents the wider operational BW of 1.5 GHz with the FBW of 51%. Compared with the other optimization methods [22], [23], higher center frequency is achieved and the performance of the DPA improves significantly by the proposed DT-SRFT optimization.

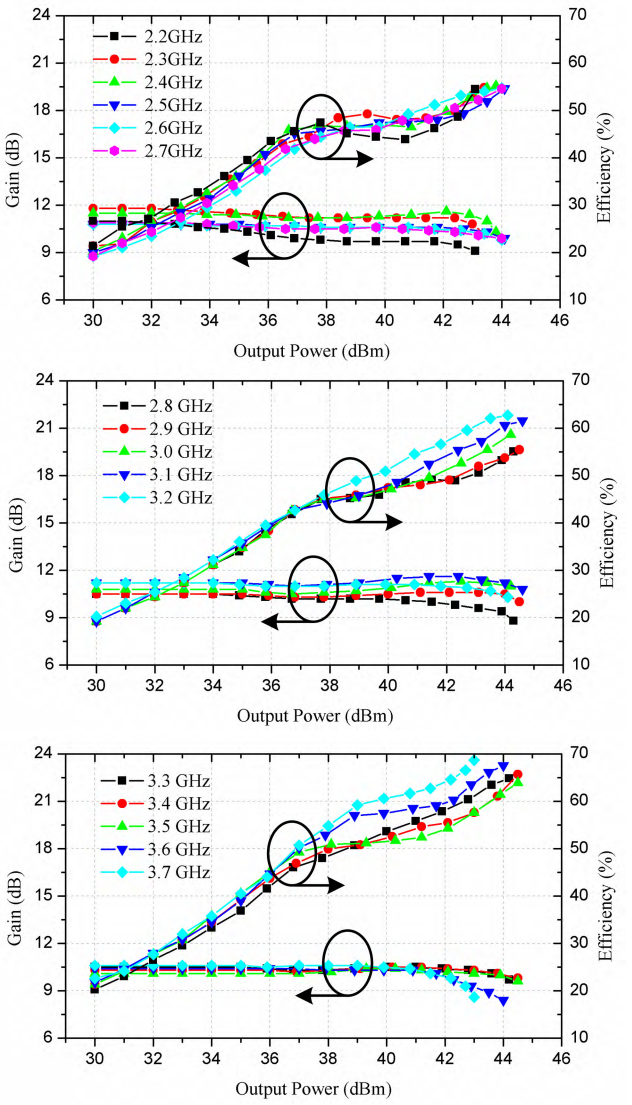

FIGURE 13. Measured gain and DE versus output power of the fabricated broadband DPA.

B. MODULATED SIGNAL MEASUREMENTS

After CW measurements, modulated signals are used to evaluate this broadband DPA in mobile communication systems. A 20-MHz LTE signal with 6.2 dB PAPR is excited to this DPA to evaluate the linearity and efficiency performances over the entire frequency band.

As shown in Fig. 15, the designed broadband DPA exhibits a 45.3%-55.9% average efficiency over the 1.5 GHz BW at 6.5-dB BO power level (36.5-38.1 dBm), while the adjacent channel leakage ratios (ACLRs) are −29.6∼-39.6 dBc. Utilizing the digital predistortion (DPD) to linearize the fabricated DPA [34], the ACLRs of the DPA are improved to −50.1∼-56.5 dBc.

In addition, various DPDs are conducted to validate the linearity performance of the DPA for the upcoming 5G communication systems. An 80 MHz LTE-Advanced (LTE-A) signal with a PAPR of 7.5 dB and a concurrent dual-

TABLE 3. Comparisons with some recently published DPAs.

Ref. (Year)	Frequency (GHz)	CF[a] (GHz)	BW (GHz)	FBW (%)	$P_{out,sat}$ (dBm)	PUF[b]	DE_{sat} (%)	DE_{6dBBO} (%)	Technique
[10] (2012)	3-3.6	3.3	0.6	18.2	43-44	1.34-1.69	55-66	38-56	Wideband Compensator
[11] (2018)	1.5-3.8	2.65	2.3	87	42.3-43.4	1.08-1.40	42-63	33-55	Bandwidth Estimation
[14] (2015)	1.7-2.6	2.15	0.9	41.9	44.6-46.3	1.75-2.58	57-66	49-60	Post-Matching
[16] (2016)	1.7-2.8	2.25	1.1	48.9	44-44.5	1.53-1.73	57-71	50-55	Integrated Compensate Line
[22] (2017)	1.5-2.4	1.95	0.9	46.2	43.1-44.4	1.21-1.63	57-74	45-56	Bayesian Optimization
[23] (2013)	2.2-2.96	2.6	0.76	29.5	39.6-41.7	0.97-1.57	50-68	40-60	SRFT Optimization
This work	**2.2-3.7**	**2.95**	**1.5**	**50.9**	**43-44.6**	**1.31-1.89**	**55-69**	**45-53**	**DT-SRFT Optimization**

[a] CF means Center Frequency
[b] PUF is defined as (measured saturation power)/(devices' nominal saturated power)*$CF^{0.25}$.

TABLE 4. Linearization results of The DPA With LTE-A signal and concurrent dual-band signal.

Signal Type	BW (MHz)	PAPR (dB)	Frequency (GHz)	Output Power (dBm)	Average Efficiency (%)	ACLR before DPD (dBc)	ACLR after DPD (dBc)
4 Carriers' LTE-A	80	7.5	2.6	36.3	43.6	-28.5/-29.3	-48.6/-48.7
4 Carriers' LTE-A	80	7.5	3.5	36.9	46.7	-30.5/-33.8	-51.0/-51.1
Concurrent dual-band LTE-A	20	8	2.6	33.1	41.6	-31.6/-32.4	-52.0/-52.5
	40		3.5	33.1		-33.6/-36.6	-50.0/-50.4

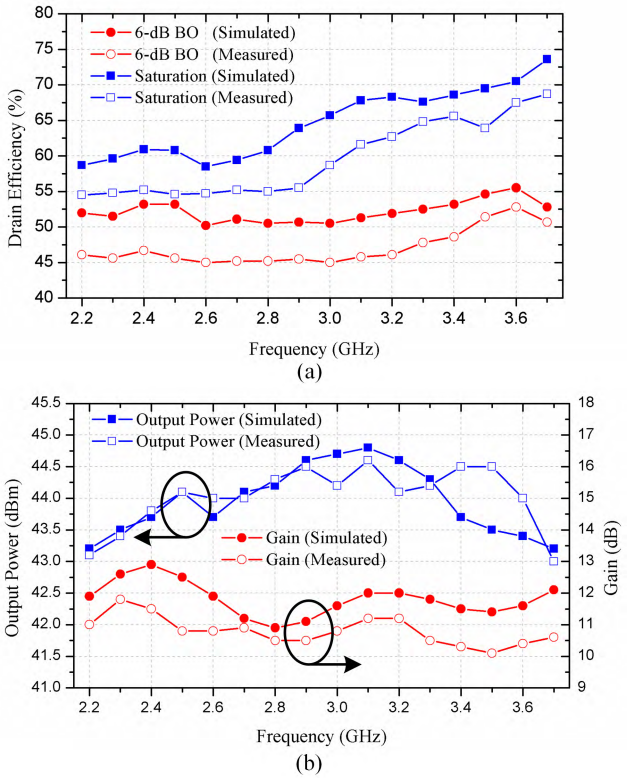

FIGURE 14. Measured and simulated frequency response of the designed DPA, including (a) DEs at 6-dB BO and saturation, (b) saturated output power and gain.

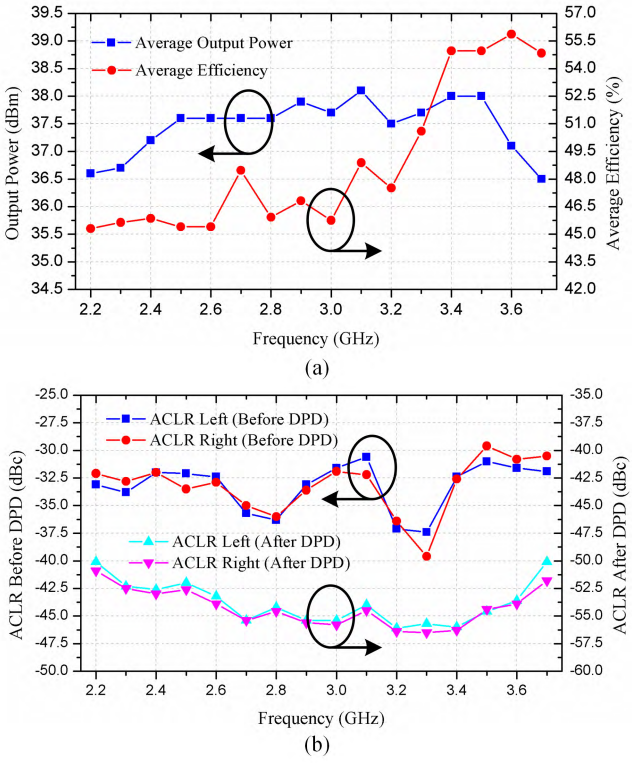

FIGURE 15. Measured results of a 6.2dB PAPR 20-MHz LTE signal, including (a) output power, average efficiency and (b) ACLR before and after DPD.

band signal with the PAPR of 8 dB and BWs of 20 and 40 MHz are employed to excite the DPA at 2.6 and 3.5 GHz to verify the DPD performance. Fig.16 and Fig. 17 show the measured output power spectral density (PSD) before and after DPD and the linearization results are summarized in Table 4. For the 80 MHz 4 carriers' LTE-A signals, when the average output power is 36.3 and 36.9 dBm, the designed DPA can achieve an efficiency of 43.6% and 46.7% with the

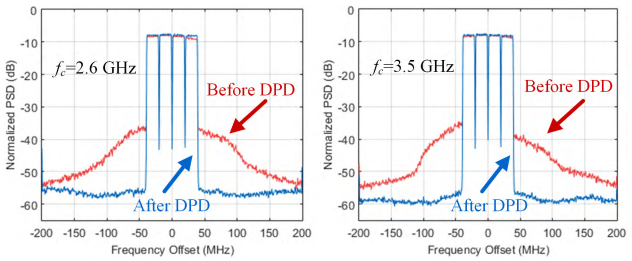

FIGURE 16. Measured output power spectral density of 80 MHz LTE-A signal before and after DPD.

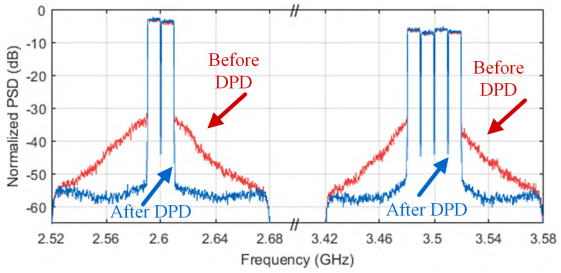

FIGURE 17. Measured output power spectral density of concurrent dual-band signal before and after DPD.

ACLRs lower than -48.6 dBc at the candidate 5G frequency bands. Excited with the concurrent dual-band LTE-A signal, the designed DPA exhibits an average efficiency of 41.6% with the total output power at 36 dBm (33 dBm in each band). The two-dimensional decomposed vector rotation-based model [35], [36] was applied to linearize the DPA. ACLRs lower than -50 dBc can be achieved for each band. The modulated signal measurement results validate the outstanding performance of the designed DPA for the current and future mobile communication systems.

V. CONCLUSION

In this paper, a novel DT-SRFT optimization is proposed to achieve the dual-impedance transformation in DPA's OMN design simultaneously. By introducing the G-DPF and united TF, a detailed process is presented in DT-SRFT to combine the optimizations of carrier and peaking OMNs together. A novel design procedure of the proposed method is introduced to simplify the broadband DPA design. For verification, a broadband DPA is designed and fabricated over 2.2-3.7 GHz. The compensating lines are eliminated to improve the performance of the DPA. CW measurement results show that the proposed DPA presents excellent output power and efficiency performances over the 1.5 GHz operational bandwidth. When excited by modulated signals, high average efficiency and good linearity are achieved across the entire frequency band. The results can validate the effectiveness of the proposed SRFT modification. The designed DPA can be employed in current LTE and upcoming 5G mobile communication systems.

REFERENCES

[1] R. Ma, K. H. Teo, S. Shinjo, K. Yamanaka, and P. M. Asbeck, "A GaN PA for 4G LTE-advanced and 5G: Meeting the telecommunication needs of various vertical sectors including automobiles, robotics, health care, factory automation, agriculture, education, and more," *IEEE Microw. Mag.*, vol. 18, no. 7, pp. 77–85, Nov./Dec. 2017.

[2] Z. Popovic, "Amping up the PA for 5G: Efficient GaN power amplifiers with dynamic supplies," *IEEE Microw. Mag.*, vol. 18, no. 3, pp. 137–149, May 2017.

[3] R. Darraji, P. Mousavi, and F. M. Ghannouchi, "Doherty goes digital: Digitally enhanced Doherty power amplifiers," *IEEE Microw. Mag.*, vol. 17, no. 8, pp. 41–51, Aug. 2016.

[4] J. Xia, X. Zhu, L. Zhang, J. Zhai, and Y. Sun, "High-efficiency GaN Doherty power amplifier for 100-MHz LTE-advanced application based on modified load modulation network," *IEEE Trans. Microw. Theory Techn.*, vol. 61, no. 8, pp. 2911–2921, Aug. 2013.

[5] W. Hallberg, M. Özen, D. Gustafsson, K. Buisman, and C. Fager, "A Doherty power amplifier design method for improved efficiency and linearity," *IEEE Trans. Microw. Theory Techn.*, vol. 64, no. 12, pp. 4491–4504, Dec. 2016.

[6] X.-H. Fang, H.-Y. Liu, and K.-K. M. Cheng, "Extended efficiency range, equal-cell Doherty amplifier design using explicit circuit model," *IEEE Micro. Compon. Lett.*, vol. 27, no. 5, pp. 497–499, May 2017.

[7] F. Meng, Y. Sun, L. Tian, and X.-W. Zhu, "A broadband high-efficiency Doherty power amplifier with continuous inverse class-F design," in *Proc. 32nd Gen. Assem. Sci. Symp. Int. Union Radio Sci. (URSI GASS)*, Montreal, QC, Canada, Aug. 2017, pp. 1–3.

[8] H. Oh *et al.*, "Doherty power amplifier based on the fundamental current ratio for asymmetric cells," *IEEE Trans. Microw. Theory Techn.*, vol. 65, no. 11, pp. 4190–4197, Nov. 2017.

[9] L. Piazzon, R. Giofrè, P. Colantonio, and F. Giannini, "A wideband Doherty architecture with 36% of fractional bandwidth," *IEEE Microw. Wireless Compon. Lett.*, vol. 23, no. 11, pp. 626–628, Nov. 2013.

[10] J. M. Rubio, J. Fang, V. Camarchia, R. Quaglia, M. Pirola, and G. Ghione, "3–3.6-GHz wideband GaN Doherty power amplifier exploiting output compensation stages," *IEEE Trans. Microw. Theory Techn.*, vol. 60, no. 8, pp. 2543–2548, Aug. 2012.

[11] J. J. M. Rubio, V. Camarchia, M. Pirola, and R. Quaglia, "Design of an 87% fractional bandwidth Doherty power amplifier supported by a simplified bandwidth estimation method," *IEEE Trans. Microw. Theory Techn.*, vol. 66, no. 3, pp. 1319–1327, Mar. 2018.

[12] R. Darraji, D. Bhaskar, T. Sharma, M. Helaoui, P. Mousavi, and F. M. Ghannouchi, "Generalized theory and design methodology of wideband Doherty amplifiers applied to the realization of an octave-bandwidth prototype," *IEEE Trans. Microw. Theory Techn.*, vol. 65, no. 8, pp. 3014–3023, Aug. 2017.

[13] R. GiofrÃÍ, L. Piazzon, P. Colantonio, and F. Giannini, "A closed-form design technique for ultra-wideband Doherty power amplifiers," *IEEE Trans. Microw. Theory Techn.*, vol. 62, no. 12, pp. 3414–3424, Dec. 2014.

[14] J. Pang, S. He, C. Huang, Z. Dai, J. Peng, and F. You, "A post-matching Doherty power amplifier employing low-order impedance inverters for broadband applications," *IEEE Trans. Microw. Theory Techn.*, vol. 63, no. 12, pp. 4061–4071, Dec. 2015.

[15] J. Xia, M. Yang, and A. Zhu, "Improved Doherty amplifier design with minimum phase delay in output matching network for wideband application," *IEEE Microw. Wireless Compon. Lett.*, vol. 26, no. 11, pp. 915–917, Nov. 2016.

[16] J. Xia, M. Yang, Y. Guo, and A. Zhu, "A broadband high-efficiency doherty power amplifier with integrated compensating reactance," *IEEE Trans. Microw. Theory Techn.*, vol. 64, no. 7, pp. 2014–2024, Jul. 2016.

[17] S. Chen, G. Wang, Z. Cheng, and Q. Xue, "A bandwidth enhanced Doherty power amplifier with a compact output combiner," *IEEE Microw. Wireless Compon. Lett.*, vol. 26, no. 6, pp. 434–436, Jun. 2016.

[18] W. Shi *et al.*, "Broadband continuous-mode Doherty power amplifiers with noninfinity peaking impedance," *IEEE Trans. Microw. Theory Techn.*, vol. 66, no. 2, pp. 1034–1046, Feb. 2018.

[19] X. Chen, W. Chen, F. M. Ghannouchi, Z. Feng, and Y. Liu, "A broadband Doherty power amplifier based on continuous-mode technology," *IEEE Trans. Microw. Theory Techn.*, vol. 64, no. 12, pp. 4505–4517, Dec. 2016.

[20] X. Chen, W. Chen, Q. Zhang, F. M. Ghannouchi, and Z. Feng, "A 200 watt broadband continuous-mode Doherty power amplifier for base-station applications," in *IEEE MTT-S Int. Microw. Symp. Dig.*, Honolulu, HI, USA, Jun. 2017, pp. 1110–1113.

[21] X. Y. Zhou, S. Y. Zheng, W. S. Chan, and D. Ho, "Efficiency enhanced post-matching Doherty power amplifier based on modified phase compensation network," in *IEEE MTT-S Int. Microw. Symp. Dig.*, Honolulu, HI, USA, Jun. 2017, pp. 785–788.
[22] P. Chen, J. Xia, B. M. Merrick, and T. J. Brazil, "Multiobjective Bayesian optimization for active load modulation in a broadband 20-W GaN Doherty power amplifier design," *IEEE Trans. Microw. Theory Techn.*, vol. 65, no. 3, pp. 860–871, Mar. 2017.
[23] G. Sun and R. H. Jansen, "Broadband Doherty power amplifier via real frequency technique," *IEEE Trans. Microw. Theory Techn.*, vol. 60, no. 1, pp. 99–111, Jan. 2012.
[24] H. J. Carlin and J. J. Komiak, "A new method of broad-band equalization applied to microwave amplifiers," *IEEE Trans. Microw. Theory Techn.*, vol. MTT-27, no. 2, pp. 93–99, Feb. 1979.
[25] H. J. Carlin, "A new approach to gain-bandwidth problems," *IEEE Trans. Circuits Syst.*, vol. CAS-24, no. 4, pp. 170–175, Apr. 1977.
[26] B. S. Yarman, *Design of Ultra Wideband Power Transfer Networks*. New York, NY, USA: Wiley, 2010.
[27] Z. Dai, S. He, F. You, J. Peng, P. Chen, and L. Dong, "A new distributed parameter broadband matching method for power amplifier via real frequency technique," *IEEE Trans. Microw. Theory Techn.*, vol. 63, no. 2, pp. 449–458, Feb. 2015.
[28] Z. Dai, S. He, J. Pang, J. Peng, C. Huang, and F. You, "Sub-optimal matching method for dual-band class-J power amplifier using real frequency technique," *IET Microw., Antennas Propag.*, vol. 11, no. 9, pp. 1218–1226, 2017.
[29] Z. Dai, S. He, J. Peng, C. Huang, W. Shi, and J. Pang, "A semianalytical matching approach for power amplifier with extended Chebyshev function and real frequency technique," *IEEE Trans. Microw. Theory Techn.*, vol. 65, no. 10, pp. 3892–3902, Oct. 2017.
[30] Y. J. Sun and X. W. Zhu, "Broadband continuous class-F^{-1} amplifier with modified harmonic-controlled network for advanced long term evolution application," *IEEE Microw. Wireless Compon. Lett.*, vol. 25, no. 4, pp. 250–252, Apr. 2015.
[31] L. Ma, J. Zhou, and W. Huang, "A broadband highly efficient harmonic-tuned power amplifier exploiting compact matching network," *IEEE Micro. Compon. Lett.*, vol. 25, no. 11, pp. 718–720, Nov. 2015.
[32] N. Tuffy, L. Guan, A. Zhu, and T. J. Brazil, "A simplified broadband design methodology for linearized high-efficiency continuous Class-F power amplifiers," *IEEE Trans. Microw. Theory Techn.*, vol. 60, no. 6, pp. 1952–1963, Jun. 2012.
[33] P. I. Richards, "Resistor-transmission-line circuits," *Proc. IRE*, vol. 36, no. 2, pp. 217–220, Feb. 1948.
[34] L. Guan and A. Zhu, "Simplified dynamic deviation reduction-based Volterra model for Doherty power amplifiers," in *Proc. IEEE Int. Integr. Nonlinear Microw. Millim.-Wave Circuits Workshop*, Vienna, Austria, Apr. 2011, pp. 1–4.
[35] N. Kelly, W. Cao, and A. Zhu, "Preparing linearity and efficiency for 5G: Digital predistortion for dual-band Doherty power amplifiers with mixed-mode carrier aggregation," *IEEE Micro. Mag.*, vol. 18, no. 1, pp. 76–84, Feb. 2017.
[36] A. Zhu, "Decomposed vector rotation-based behavioral modeling for digital predistortion of RF power amplifiers," *IEEE Trans. Microw. Theory Techn.*, vol. 63, no. 2, pp. 737–744, Feb. 2015.

FAN MENG (S'14) received the B.S. degree in information science and engineering from Southeast University, Nanjing, China, in 2011, where he is currently pursuing the Ph.D. degree with the State Key Laboratory of Millimeter Waves.

His current research interests include highly linear and efficient microwave PA design and high efficient Doherty and supply modulated PA design.

XIAO-WEI ZHU (S'88–M'95) received the M.E. and Ph.D. degrees in radio engineering from Southeast University, Nanjing, China, in 1996 and 2000, respectively.

Since 1984, he has been with Southeast University, where he is currently a Professor with the School of Information Science and Engineering. He has authored or co-authored over 90 technical publications. He holds 15 patents. His research interests include RF and antenna technologies for wireless communications, microwave and millimeter-wave theory and technology, and power amplifier nonlinear character and its linearization research with a particular emphasis on wideband and high-efficiency GaN PAs.

Dr. Zhu is the President of the Microwave Integrated Circuits and Mobile Communication Sub-Society and the Microwave Society of CIE, and the Secretary of the IEEE MTT-S/AP-S/EMC-S Joint Nanjing Chapter. He was a recipient of the 1994 First-Class Science and Technology Progress Prize presented by the Ministry of Education of China and the 2003 Second-Class Science and Technology Progress Prize of Jiangsu Province, China.

JING XIA (S'12–M'15) received the M.E. degree in computer science and technology from Jiangsu University, Jiangsu, China, in 2007, and the Ph.D. degree in electromagnetic field and microwave technology from Southeast University, Nanjing, China, in 2014.

From 2015 to 2016, he was a Post-Doctoral Research Fellow with the RF and Microwave Research Group, University College Dublin, Dublin, Ireland. He is currently an Associate Professor with the School of Computer Science and Communication Engineering, Jiangsu University, Zhenjiang, China. His recent research is focused on high back-off efficiency power amplifier (PA) design, wideband efficient PA design, and digital pre-distortion techniques.

CHAO YU (S'09–M'15) received the B.E. degree in information engineering and the M.E. degree in electromagnetic fields and microwave technology from Southeast University, Nanjing, China, in 2007 and 2010, respectively, and the Ph.D. degree in electronic engineering from University College Dublin, Dublin, Ireland, in 2014.

He is currently an Associate Professor with the State Key Laboratory of Millimeter Waves, School of Information Science and Engineering, Southeast University. His research interests include microwave and millimeter-wave power amplifier modeling and linearization, and 5G massive MIMO RF system design.